Iraqi Journal of Physics, 2025 ***Vol. 23, No.2, PP.128-137***
https://doi.org/10.30723/ijp.vxxixx. ***P-ISSN: 2070-4003***
E-ISSN: 2664-5548

Preparation of Hybrid Light-Emitting Diodes (OI-LED) Based on Carbon Nanoparticles

Hussein Riyadh Mohammed[1*] **and Asama N. Naje**[1]
[1]*Department of Physics, College of Science, University of Baghdad, Iraq*
[*]Corresponding author: hussieni6762@gmail.com

Abstract

A hybrid organic-inorganic light-emitting diode (OI-LED) device was made by combining carbon nanoparticles (CNPs) that are 20 to 40 nm in size with layers of organic and inorganic semiconductors. This technique resulted in enhanced electroluminescence (EL) generation. The active layer comprised a composite of poly[(9,9-dioctylfluorenyl-2,7-diyl)-co-(4,4′-(N-(4-sec-butylphenyl) diphenylamine))] (TFB) and tris(8-quinolinolato) aluminum(III) (Alq_3). The device fabrication included spin-coating and phase-segregation techniques, yielding a thin-film structure with ITO/TFB/CNP/Alq_3/Al configuration. The electroluminescent characteristics of the fabricated organic light-emitting diode were analysed by evaluating performance variations at different bias voltages (8, 9, and 10 V) and modifying the organic layers' deposition parameters at room temperature. Current-voltage curves exhibited a pronounced knee voltage of 0.6 V, significantly influenced by the applied bias voltage. This characteristic enabled the OI-LED to emit a broad light spectrum ranging from 300 to 800 nm. Electronic transitions associated with the surface states and sub-levels within the CNPs are responsible for the broad emission spectrum. The analysis of colour space, employing the Commission Internationale de l'Éclairage (CIE) standard, revealed that the device's correlated colour temperature (CCT) ranged from 1550 to 2550 K.

Article Info.

Keywords:
Electroluminescence (EL), Organic-Inorganic Light-Emitting Diode (OI-LED), Hybrid Light-Emitting Diode (HLED), Trifluorobenzene (TFB), Carbon Nanoparticles (CNPs).

Article history:
Received: Mar.31,2024
Revised: Dec. 25, 2024
Accepted: Jan. 02, 2025
Published: Jun. 01,2025

1. Introduction

Silicon and germanium, as well as their alloys, have historically been significant in numerous industrial applications [1]. In the late 1960s, Heeger, MacDiarmid, and Shirakawa achieved a significant breakthrough by demonstrating the electrical conductivity of doped polyethylene, a conductive polymer, which earned them the Nobel Prize [2]. Extensive study in semiconductor physics, a fundamental aspect of modern technology, has led to the advancement of high-performance organic semiconductors, greatly transforming in the realm of electronic devices [3,4]. These improvements have generated significant anticipation for their extensive application in essential technologies such as light-emitting diodes (LEDs), solar cells, flexible displays, detectors, and sensors [5]. Organic Light-Emitting Diodes (OLEDs) have attracted significant scientific interest due to their potential for high-intensity, flat-panel display applications. Significant efforts have been focused on enhancing OLED achievement by tackling key challenges, such as injection barriers at the interfaces between organic materials and high-performance electrodes [6].

Organic materials comprise a wide category of solid substances defined by interconnected molecular structures, such as polymers. These materials predominantly comprise carbon and hydrogen atoms, with the possible inclusion of nitrogen and other elements. Organic semiconductors display an energy bandgap typically ranging from 2 to 4 eV [7]. Initially, these materials were erroneously classified as insulators. However, their intrinsic semiconducting properties can be realised with the introduction of charge carriers by electrodes or doping techniques. Advancements in nanoscience, and nanotechnology have profoundly enhanced our comprehension of semiconductor behavior at the nano scale, uncovering distinctive features in materials like metal oxides and carbon compounds. Elemental carbon displays properties including low solubility in water, restricted chemical reactivity, and minimal photoluminescence [8]. The utilization of chemical and physical methods to fabricate carbon nanostructures, including graphene quantum dots (GQDs), carbon nanoparticles (CNPs), single-walled carbon nanotubes (SWCNTs), and multi-walled carbon nanotubes (MWCNTs), has converted carbon from an insulator into a functional semiconductor material [9]. These carbon nanocomposites exhibit increased solubility, chemical reactivity, and enhanced photoluminescence, presenting considerable potential for the advancement of inorganic light-emitting diodes [10].

Electroluminescence can be achieved by fabricating hybrid LEDs that combine thin-film layers of both organic, and inorganic substances. The layered structures are positioned between two electrodes, one of which must be transparent. To enhance effective charge injection and transport to the CNP light-emitting layer, supplementary layers are integrated, comprising hole-transporting layers (HTLs), hole-injection layers (HILs), electron-transporting layers (ETLs), and electron-injection layers (EILs) [11,12]. Moreover, CNPs substantially boost device performance owing to the existence of surface state levels and sublevels that promote effective light emission [13,14].

This study investigates the utilization of Poly[(9,9-dioctylfluorenyl-2,7-diyl)-co-(4,4′-(N-(4-sec-butylphenyl)diphenylamine))] (TFB) in conjunction with carbon nanoparticles to enhance the hole-injection layer (HIL) capabilities within hybrid LED photovoltaic cells. Furthermore, the electron-injection layer (EIL) comprising tris(8-hydroxyquinolinato)aluminum (Alq_3), renowned for its high thermal stability, plays a crucial role in determining the emission level [15,16]. Organic-inorganic LEDs (OI-LEDs) offer a compelling platform for device applications, characterized by numerous advantages including lightweight construction, extensive coverage, high flexibility, transparence, and cost efficiency. Attributes are realized through thin-film deposition techniques such as vacuum thermal evaporation and spin coating. The method is explained in detail by Haiping [4]. This study comprehensively examined the optical and electrical properties of the fabricated devices. The photoluminescence energy gap of all materials was determined using Planck's equation [17]. Subsequently, the correlated color temperature (CCT) was calculated based on the CIE 1931 chromaticity coordinates (x', y'), where x' and y' represent the relative contributions of red and green colors, respectively.

$$x' = \frac{A}{A+B+C} \tag{1}$$

$$y' = \frac{B}{A+B+C} \tag{2}$$

A, B, and C represent the areas beneath the curve corresponding to the red, green, and blue parts of the electromagnetic spectrum, respectively. The correlated colour temperature (CCT) of light is determined via McCamy’s approximation polynomial for estimating the CCT from the x', and y' chromaticity coordinates, as expressed in Eq.(3) [18,19]:

$$\mathrm{CCT} = -449(n^3) + 3525(n^2) - 6823\,(n) + 5520.33 \tag{3}$$

where

$$n = \frac{x'-0.332}{y'-0.1855} \tag{4}$$

The aim of the research was to enhance the intensity of organic light-emitting diodes by incorporating carbon nanostructures. These nanostructures contribute to the formation of multiple surface and sub-state levels, facilitating electronic and vibrational transitions, which resulted in a broad spectrum of light emissions.

2. Experimental Work

The experimental protocol encompassed the subsequent steps: 10 mg of poly [(9,9-dioctylfluorenyl-2,7-diyl)-co-(4,4′-(N-(4-sec-butylphenyl)diphenylamine))] (TFB) was solubilized in 1 mL of chloroform utilizing an ultrasonic bath with a magnetic stirrer [20]. Subsequently, CNPs were integrated into the TFB solution at a weight ratio of x/300, with x denoting the weight of TFB. Independently, 30 mg of tris(8-hydroxyquinolinato)aluminum (Alq_3) was solubilized in 3 mL of ethanol, a solvent that neither interacts with nor degrades TFB. The dispersion process utilized the same ultrasonic bath and magnetic stirring methods as previously employed mentioned earlier by Kadim et al [21]. A final coating was coated on a 2 × 2 cm conducting indium tin oxide (ITO) substrate using the spin-coating process after the solutions were prepared.

The TFB:CNP blend layer was then applied to the ITO substrate using spin-coating at 2000 rpm, and subsequently dried at 50°C for one hour. The Alq_3 layer was ultimately coated onto the TFB:CNP layer using the same spin-coating parameters as the work of Mohammed and Naje [22], as illustrated in Fig.1.

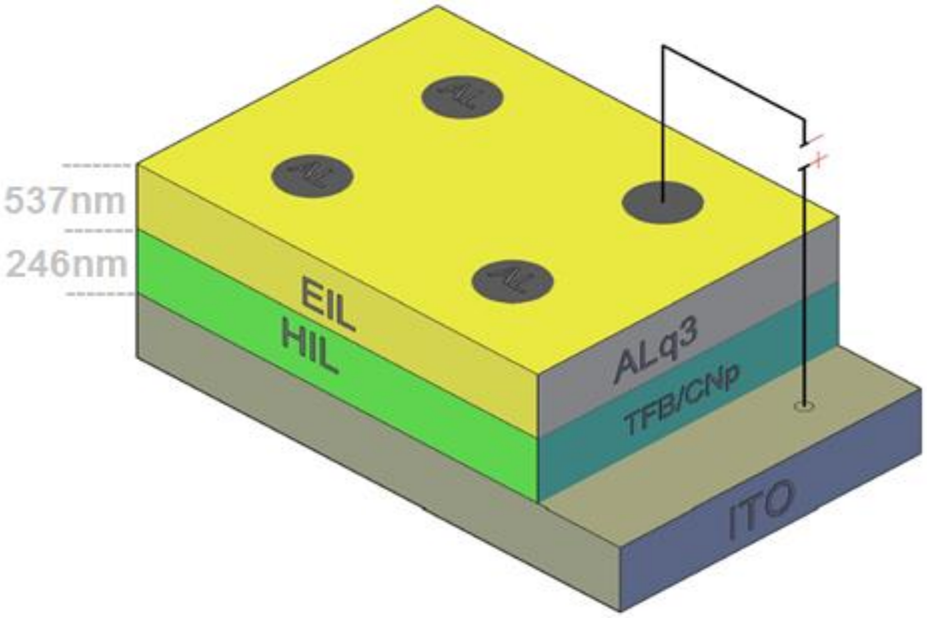

Figure 1: Schematic diagram of multilayers device

3. Results and Discussion

3.1 Optical properties (Absorbance and Photoluminescence)

The absorption spectra of the solutions (TFB in chloroform, CNPs in chloroform, and Alq_3 in ethanol) were analyzed within the wavelength range of 300-800 nm, as illustrated in Fig.2(a-c). All solutions displayed absorption peaks in the near-ultraviolet region, subsequently followed by a progressive decrease in absorbance with increasing wavelength. The peak absorption maxima for TFB, Alq_3, and CNPs were recorded at 428, 396, and 290 nm, respectively [23]. Subsequently, the wavelengths of 428, 396, and 290 nm were utilized as excitation sources to assess the photoluminescence (PL) spectra of the respective solutions, as depicted in the Fig.2. Energy band gap of each material was ascertained utilising Planck's equation. The initial photoluminescence emission peak of TFB, located at 477 nm, corresponds to the electronic transition from the lowest unoccupied molecular orbital (LUMO) to the highest occupied molecular orbital (HOMO), signifying an energy difference of roughly 2.6 eV. In a similar manner for Alq_3, the initial photoluminescence emission peak at 520 nm indicates the transition from the LUMO to the HOMO, yielding an energy bandgap of roughly 2.38 eV [24]. Energy bandgap for the CNPs was determined to be approximately 2 eV, corresponding to the band-to-band transition seen at a wavelength of 620 nm [25].

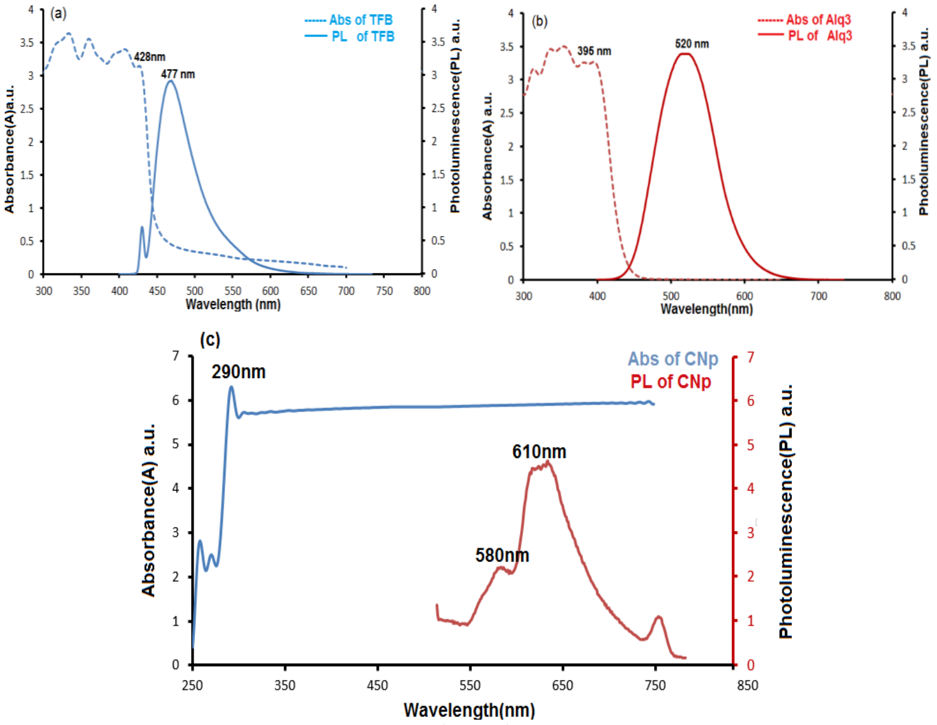

Figure 2: Absorbance and Photoluminescence (a) TFB (b) Alq_3 and (c) CNp.

3.2 Morphological Properties (Scanning Electron Microscope (SEM))

The resulting structure was a multilayered film (ITO/TFB/CNP/Alq_3/AL). A cross-section, examined using a scanning electron microscope (MIRA3 TESCAN), revealed a total thickness of approximately 783 nm, as shown in Fig.3 with magnification power (135kx). The first layer, consisting of TFB mixed with CNP, had a thickness of 264 nm, while the second layer, composed of Alq_3, measured 537 nm in thickness.

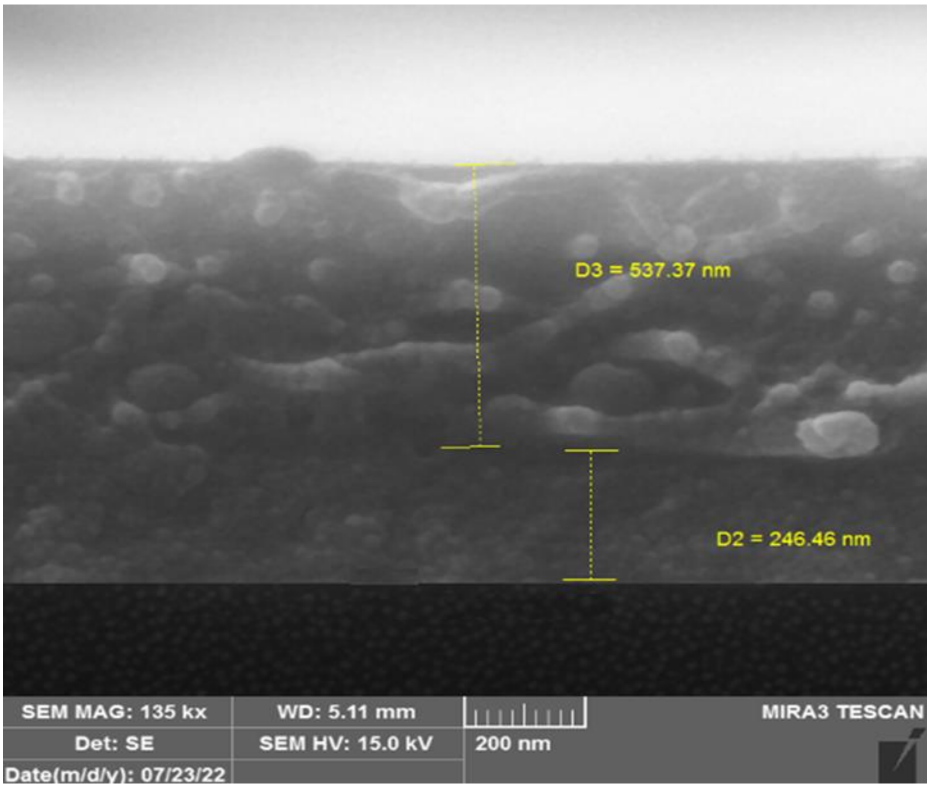

Figure 3: Scanning Electron Microscope cross section with 135kx for device.

3.3 Electrical properties (Current-Voltage Properties)

The current-voltage (I-V) properties of a typical organic-inorganic LED device (ITO/TFB/CNP/Alq_3/AL) were assessed at room temperature (RT), as depicted in Fig. 4. The current behavior can be classified into three main regimes. In the initial regime (<2 V), the current has a linear relationship with voltage ($I \propto V$), signifying carrier transport via low-voltage tunneling mechanisms. A consistent knee voltage of 0.6 V is noted in this regime, while the turn-on voltage is ascertained to be 1.57 V. The second regime (2-8 V) exhibits an exponential rise in current relative to the applied voltage, defined by the formula $I \propto \exp(XV)$, where X is 0.316.

The carriers introduced into the dielectric are produced by the thermionic process occurring at the barrier. Consequently, the quantity of free charges is significantly less than that of trapped charges, and the current exhibits an exponential correlation with the voltage. Fowler–Nordheim tunneling may occur alongside thermionic emission. Voltage levels of 8 V are deemed to be inside the fill factor voltage range (VLFR). The prolonged duration of the second regime can be ascribed to the comparatively limited carrier mobility inherent in organic materials [21,26]. In the third regime (>8 V), the current-voltage relationship demonstrates a power-law dependence ($I \propto V^X$), with X equal to 0.625. This regime signifies the initiation of light emission, as an elevation in the bias voltage across the device results in a greater density of injected charge carriers within the excited states of the organic layers. This increased carrier concentration subsequently amplifies Coulombic interactions, leading to the emission of a wide range of wavelengths [22].

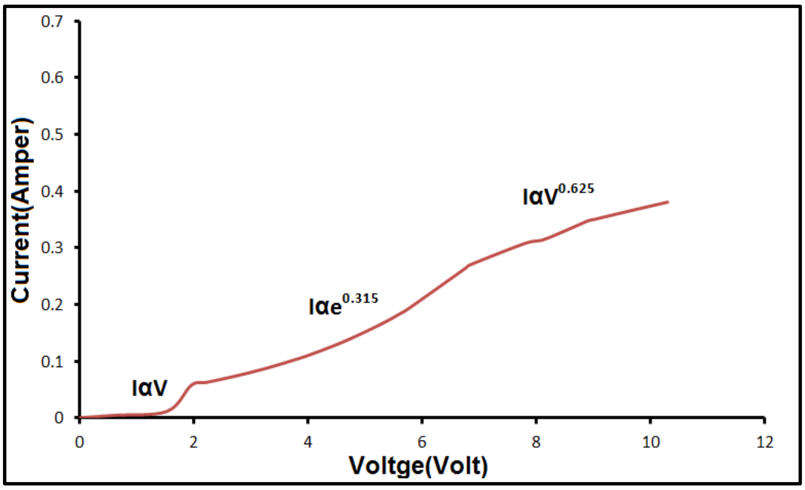

Figure 4: I-V properties of multilayer devices.

3.4 Electroluminesces Measurements

Electroluminescence (EL) measurements were performed at forward bias voltages of 8, 9, and 10 V, with the emitted light traversing the sample. The emission spectra of the hybrid device was obtained utilising a photomultiplier tube detector at room temperature (RT) (Instrument model: RF-5301PC, Light source: 150 W Xenon lamp, Diffraction grating density: 1300 lines/mm, Wavelength accuracy: ±1.5 nm). TFB served as the hole transport layer, while Alq_3 functioned as the electron transport layer. The indium tin oxide anode enables the passage of holes into HOMO for TFB, and the valence band (VB) of CNPs. In contrast, the aluminium cathode promotes the injection, and transit of electrons into LUMO of Alq_3, and the conduction band (CB) of the CNPs. Charge recombination occurs due to Coulombic attraction resulting from the injection and subsequent transit of holes and electrons across the organic layers, as depicted in Fig.5. The recombination process generates excitons, and exciplexes, culminating in the emission of a broad spectrum of light from the ITO/TFB/CNP/Alq_3/AL device.

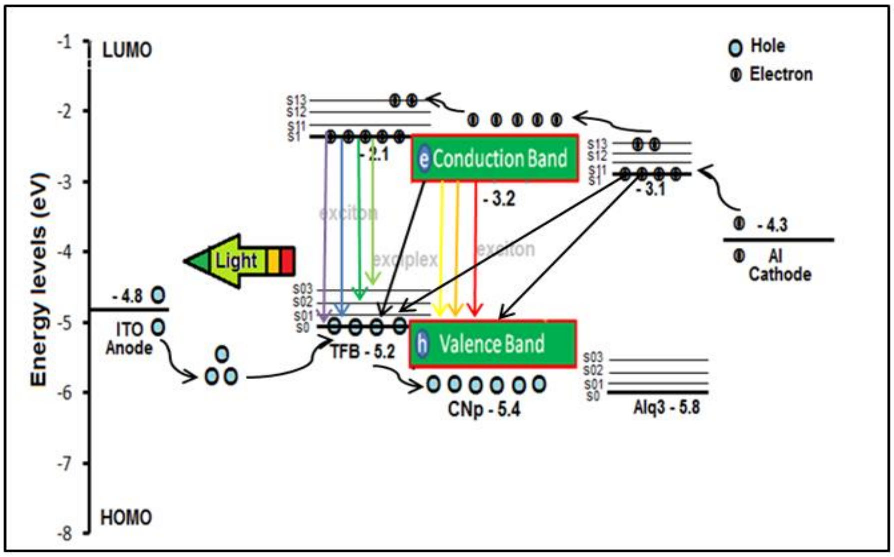

Figure5: Energy levels of a multilayer device ITO /TFB/CNp/Alq_3/AL[1,2,4,13,25,26].

The observed emission spectrum of the hybrid device, as illustrated in Fig.6, demonstrates a significant enhancement, broadening, and an increase in intensity compared to the previously fabricated OLED device (ITO/PEDOT:PSS/TFB/Alq_3/AL)

[22]. This enhancement is attributed to the incorporation of CNPs as an interlayer within the device architecture. The presence of surface states and sub-levels within the CNPs contributes to a red-shift in the emission peak, extending the emission spectrum into the yellow, orange, and red regions. The emission spectra were acquired under forward bias voltages of 8, 9, and 10 V. Three distinct spectral features were identified: (i) emission peaks observed at 378, 427, 450, and 463 nm, resulting from electronic transitions between the HOMO and LUMO levels of the TFB compound, associated with the formation of exactions within the TFB layer; (ii) a series of dominant emission peaks at 497, 505, 506, 550, 569, and 580 nm, attributed to electronic transitions between the valence band (VB) and conduction band (CB) of the CNPs, facilitated by the presence of surface states and sub-levels; and (iii) emission peaks at 596, 601, 631, 639, 679, and 686 nm, arising from the formation of exciplexes between the CB of the CNPs and the HOMO level of the TFB. The observed emission peak at 737 nm is tentatively attributed to electronic transitions between the LUMO level of one of the organic compounds and the sub-levels within the CNPs.

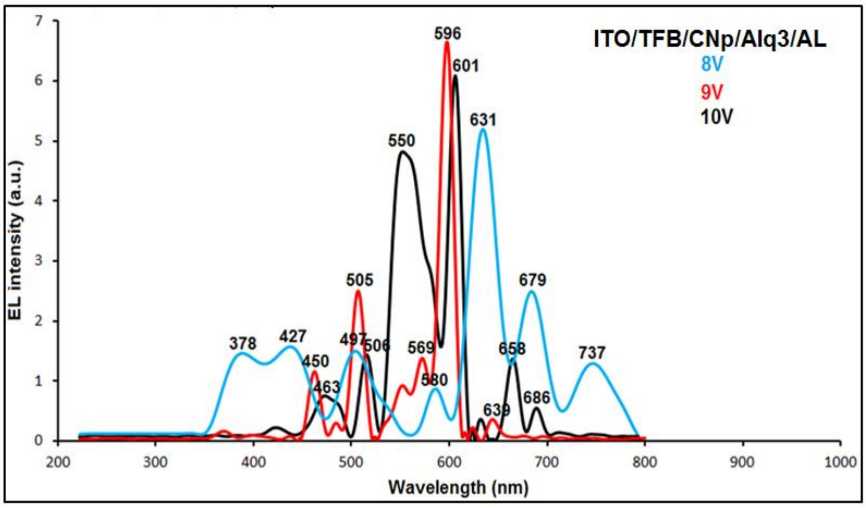

Figure 6: EL at different bias forward voltages.

EL data are presented in Fig.7 utilising the colour of light according to the Commission Internationale de l'Éclairage (CIE) 1931 chromaticity coordinates, where the colour coordinates x' and y' were derived from Eqs. (1) and (2), while the correlated colour temperature (CCT) and the colour slope (n) were computed from Eqs. (3) and (4), as detailed in Table 1. Monochromaticity was obtained in the device within the red spectrum region despite the change in bias voltage. The spectrum of broadband EL emission encompasses nearly the entirety of the visible spectrum, whereas the calculations pertaining to CCT are significantly confined to the region of the red spectrum. This phenomenon is ascribed to the pronounced intensity observed in the red regions, which is a consequence of the existence of surface state levels and sublevels for Carbon nanoparticles.

The resultant of CCT and coordinates (x' ,y') are illustrated in Table 1.

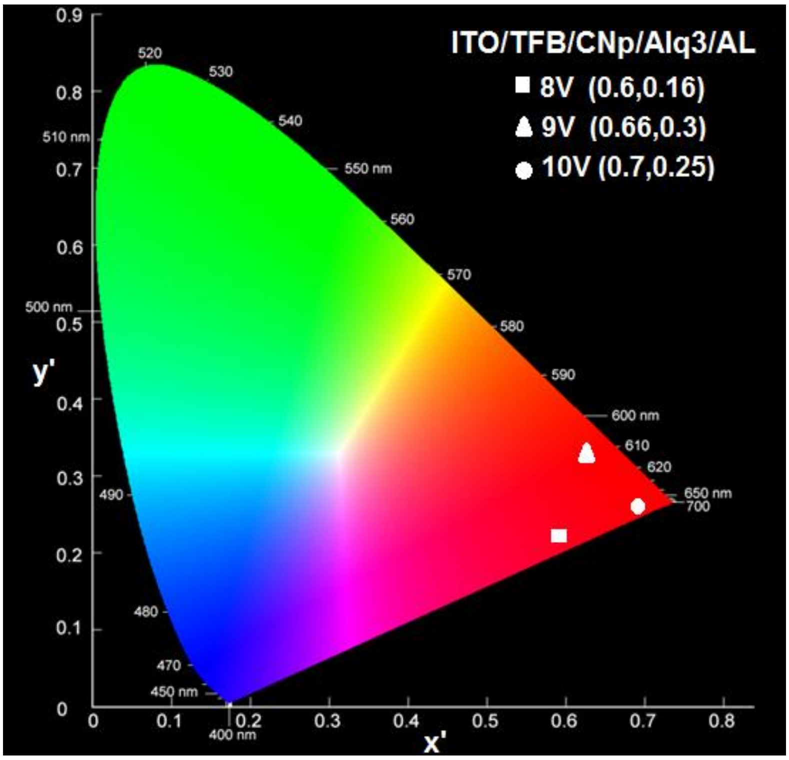

Figure 7: Shows the seven coordinates of a multilayer device of the CIE 1931 chromaticity diagram.

Table 1: CCT and x' and y' coordinates for bias forward voltages of the ITO/TFB/CNP/Alq$_3$/AL sample.

Voltage (V)	(*x'*, *y'*)	*n*	CCT (K)
8	(0.6, 0.16)	0.8064	2052
9	(0.66, 0.3)	0.6454	2176
10	(0.7, 0.25)	1.5877	1302

4. Conclusions

This study developed a multi-wavelength source utilising a hybrid LED composed of organic (TFB, and ALq$_3$) and inorganic (CNP) multilayered thin films, functioning at different forward bias voltages (8, 9, and 10 V). This occurs through the transition between the HOMO, and LUMO levels of the organic layer or between the conduction band (CB), and valence band (VB) of the CNPs, resulting in the formation of an exciton, whereas the electroluminescence (EL) arises from transitions between the CB, and LUMO, leading to the formation of an exciplex. A notable outcome was the enhancement of the electroluminescence of the organic LED with the incorporation of carbon nanoparticles, despite the most efficient diodes being those that produce a light source at elevated temperatures, necessitating the usage of certain nanomaterials to enhance colour purity. This signifies that all organic layers have transferred their energy to the nanomaterial layer.It resulted in achieving monochromaticity in the red spectrum region as per EL measurements and CCT.

Conflict of Interest

The authors declare that they have no conflict of interest.

References

1- Brütting, Wolfgang. "*Introduction to the physics of organic semiconductors*." Physics of organic semiconductors (2005): 1-14.

2- Lakshmanan, Raja, and SCG Kiruba Daniel. "*Engineered nanomaterials for organic light-emitting diodes (OLEDs)*." In Handbook of nanomaterials for industrial applications, pp. 312-323. Elsevier, 2018.
3- Lüssem, Björn, Moritz Riede, and Karl Leo. "*Doping of organic semiconductors.*" physica status solidi (a) 210, no. 1 (2013): 9-43.
4- He, Haiping. "Applications in OLED and QLED." *In Solution Processed Metal Oxide* Thin Films for Electronic Applications, pp. 141-154. Elsevier, 2020.
5- Will, Paul-Anton, and Sebastian Reineke. "*Organic light-emitting diodes*." In Handbook of Organic Materials for Electronic and Photonic Devices, pp. 695-726. Woodhead Publishing, 2019.
6- Gather, Malte C., Anne Köhnen, and Klaus Meerholz. "White organic light-emitting diodes." Advanced Materials 23, no. 2 (2011): 233-248.
7- Geffroy, Bernard, Philippe Le Roy, and Christophe Prat. "*Organic light-emitting diode (OLED) technology: materials, devices and display technologies*." Polymer international 55, no. 6 (2006): 572-582.
8- Wang, Youfu, and Aiguo Hu. "*Carbon quantum dots: synthesis, properties and applications*." Journal of Materials Chemistry C 2, no. 34 (2014): 6921-6939.
9- Hamid Abd, A., and Adnan Ibrahim. "O. *Synthesis of Carbon Quantum Dot by Electro-Chemical Method and Studying Optical Electrical and Structural Properties*." Chem. Methodol, 6 (2022): 823.
10-Mohammed, Aya H., and Asama N. Naje. "*Photoconductive Detector Based on Graphene Doping with Silver Nanoparticles*." Iraqi Journal of Science (2022): 5218-5231.
11- Li, Peicheng, and Zheng-Hong Lu. "*Interface Engineering in Organic Electronics: Energy-Level Alignment and Charge Transport*." Small Science 1, no. 1 (2021): 2000015.
12- Farinola, Gianluca M., and Roberta Ragni. "*Electroluminescent materials for white organic light emitting diodes*." Chemical Society Reviews 40, no. 7 (2011): 3467-3482.
13-Rodrigues, Aline Renata Novais, Wesley Renzi, Neusmar Junior Artico Cordeiro, Edson Laureto, Ivan Frederico Lupiano Dias, and José Leonil Duarte. "*Study of energy transfer in polymer blends of TFB: P3HT."* Semina: Exact and Technological Sciences 38, no. 1: 91-100 (20217) .
14- Dediu, V. Alek, Luis E. Hueso, Ilaria Bergenti, and Carlo Taliani. "*Spin routes in organic semiconductors.*" Nature materials 8, no. 9 (2009): 707-716.
15- Mohammed, Hussein Riyadh, and Omar A. Ibrahim. "*Electroluminescence of Light-Emitting Organic Semiconductor/Europium Oxide Nanoparticle Hybrid Junction.*" Iraqi Journal of Science (2020): 1952-1959.
16- Mohammed, Hussein Riyadh, and Omar A. Ibrahim. "*Preparation of Hybrid Junction Light Emitting Device from Cadmium Sulphite Quantum dot/poly-TPD Junction*." University of Thi-Qar Journal of Science 8, no. 2 (2021): 100-103.
17 - Aita, Carolyn Rubin, Ying-Li Liu, Mei Lee Kao, and Steven D. Hansen. "Optical behavior of sputter-deposited vanadium pentoxide." Journal of applied physics 60, no. 2 (1986): 749-753.
18- C.S. McCamy, "Correlated color temperature as an explicit function of chromaticity coordinates", Color Research & Application Volume, Vol.17, No.2, pp.142-144, (1992).
19- Naje, Asama N., Omar A. Ibrahim, and Estabraq T. Abdullah. "Blue Organic-Inorganic Light Emitting Diode Based on Electroluminescence CdS Nanoparticle." Iraqi Journal of Science (2023): 6277-6284.
20 - Mohammed, Hussein Riyadh. "*Fabrication of electroluminescence device for PEDOT: PSS/ploy TPD/Eu2O3 nanoparticles junction*." Iraqi Journal of Physics 17, no. 43 (2019): 33-40.
21-Kadim, Akeel M., Omar A. Ibrahim, and Wasan R. Saleh. "*Electroluminescence devices from quantum dots with TPD polymer white light generation.*" Journal of Nano Research 48 (2017): 104-113.
22- Mohammed, Hussein Riyadh, and Asama N. Naje. "*Electroluminescence of organic poly-TFB/Alq3 light-emitting device.*" Journal of Optics (2024): 1-6.
23- Wang, Zhibin, Naizhong Jiang, Menglong Liu, Ruidan Zhang, Feng Huang, and Daqin Chen. "*Bright Electroluminescent White-Light-Emitting Diodes Based on Carbon Dots with Tunable Correlated Color Temperature Enabled by Aggregation*." Small 17, no. 52 (2021): 2104551.
24- Auer-Berger, Manuel, Roman Trattnig, Tianshi Qin, Raphael Schlesinger, Marco V. Nardi, Giovanni Ligorio, Christos Christodoulou et al. "*All-solution-processed multilayer polymer/dendrimer light emitting diodes*." Organic Electronics 35 (2016): 164-170.
25- Lee, Jiun-Haw, Chia-Hsun Chen, Pei-Hsi Lee, Hung-Yi Lin, Man-kit Leung, Tien-Lung Chiu, and Chi-Feng Lin. "*Blue organic light-emitting diodes: current status, challenges, and future outlook.*" Journal of Materials Chemistry C 7, no. 20 (2019): 5874-5888.
26- Xiao, Peng, Ting Dong, Jianing Xie, Dongxiang Luo, Jian Yuan, and Baiquan Liu. "*Emergence of white organic light-emitting diodes based on thermally activated delayed fluorescence*." Applied Sciences 8, no. 2 (2018): 299.

تحضير الثنائيات الهجينة الباعثة للضوء (*OI-LED*) المعتمدة على جسيمات الكربون النانوية

حسين رضا محمد[1] واسامة ناطق ناجي[1]
[1]قسم الفيزياء، كلية العلوم، جامعة بغداد، بغداد، العراق

الخلاصة

تم إنشاء جهاز OI-LED من خلال استخدام مزيج من أشباه الموصلات العضوية وغير العضوية مرتبة في طبقات متعددة. وقد أدى ذلك إلى توليد معزز للتألق الكهربي (EL) من خلال دمج جسيمات الكربون النانوية (CNp) (يتراوح حجمها بين 20-40 نانومتر) في مواد مثل poly[(9,9-dioctylfluorenyl-2,7-diyl)-co-(4,4′-(N-(4-sec-butylphenyl)diphenylamine)] (TFB) و Tris(8-quinolinolato)aluminum(III) (Alq$_3$). تضمنت إجراءات التصنيع تطبيق طريقة الطلاء الدوراني وتقنية فصل الطور، مما أدى إلى بنية غشاء رقيق: (ITO/TFB/CNp/Alq$_3$/AL). وقد تم تحليل الخصائص الكهربية لـ OI-LED من خلال تقييم الاختلافات الناجمة عن الفولتية المتحيزة المختلفة (8، 9، و10 فولت) وترسب طبقات عضوية متنوعة في درجة حرارة الغرفة (RT). يوضح المنحنى IV بوضوح تأثير الجهد المطبق على الفولتية الركبة البالغة 1.6 فولت التي لوحظت في العينة. سمحت هذه السمات لـ OI-LED بإنتاج مجموعة واسعة من الضوء تشمل أطوال موجية من من 300 إلى 800 نانومتر، تم حساب مساحات الألوان وفحصها باستخدام نظام Commission Internationale de l'Éclairage (Cie) لعام 1931، حيث تم تحديد أن درجة حرارة اللون المرتبطة (CCT) للجهاز تتراوح من 1550 إلى 2550 كلفن.

الكلمات المفتاحيه: التلألؤ الكهربائي، الصمام الثنائي العضوي غير العضوي الباعث للضوء، الصمام الثنائي الباعث للضوء الهجين ، ثلاثي فلوروبنزين، الجسيمات النانوية الكربونية.